Control of Femtosecond Laser Ablation of Thin Films from a Dielectric Surface by Nonlinear Interaction with the Substrate

Laurent Mercadier, David M. Rayner,* and Paul B. Corkum†

Joint University of Ottawa/National Research Council Laboratory for Attosecond Science, 100 Sussex Drive, Ottawa, Ontario K1A 0R6, Canada

(Received 17 April 2014; published 2 September 2014)

Controlling the interaction of an ultrafast laser pulse with a thin film remains a difficult task, especially when aiming to confine material modifications to subwavelength scales. We introduce a method to achieve reproducible submicron ablation of thin films from a dielectric surface, in a back-irradiation geometry. First, the pulse of 45-fs duration and 800-nm central wavelength nonlinearly interacts with the dielectric and undergoes strong but reproducible modifications of its intensity profile. Then, the pulse ablates a thin polymer film [four bilayers of poly(allylamine hydrochloride) and poly(sodium 4-styrene-sulfonate), 8 nm thick] from the back surface. We measure the hole with atomic force microscopy and study the influence of laser energy and focal plane position. The radius of the resulting hole is determined by a threshold intensity for ablation. Therefore, we also demonstrate how measuring the radius as a function of focal plane position provides a new approach to profiling a tightly focused laser beam under nonlinear propagation conditions. We compare the beam profile with that predicted by a widely used propagation model and show that the latter can semiquantitatively be applied to estimate the size of achievable holes.

DOI: 10.1103/PhysRevApplied.2.034001

I. INTRODUCTION

Ultrafast laser pulse interactions with matter are key to emerging photonic applications such as micro- and nanometer-scale dielectric modifications, nanostructure formation, or 3D photonic devices fabrication [1,2]. Nanofabrication is often concerned with layered structures and thin films, and there is a significant interest in using short pulsed lasers to pattern such films using both front and back-side irradiation [3–6]. However, controlling the deposition of laser energy in a thin film remains a challenging task [7,8], not only in terms of spatial resolution but also because of the natural limitation of energy density achievable in the material. Because of its multiphoton nature, the interaction strongly depends on intensity, a property that can be used to confine absorption to the subwavelength scale. One way to achieve such small-scale modifications is to tightly focus a Gaussian beam with an intensity close to the breakdown threshold for ablation of the film [1]. However, in practical situations, even small laser energy fluctuations can have significant effects on energy absorption, so that pulse-to-pulse reproducibility can be difficult to achieve. One solution is to apply a burst of pulses; by taking into account the pulse energy fluctuations, the size of the ablated film is determined by the most energetic pulse among the total number applied [7], ensuring reproducibility from one site to another.

Here, we present a method for controlling the ablation of a thin film from a dielectric substrate with submicron precision and single-pulse irradiation. It takes advantage of the nonlinear interactions of the beam with the substrate prior to film ablation, in rear surface irradiation geometry. The idea is suggested by the carrotlike shape of the damage induced after multiple irradiations in wide-band-gap materials [9]. The beam profile is altered in such a way that high intensity in the tail is confined in a subwavelength region, so it is important to test if this "tail" can be used to desorb or ablate the films.

It is well known that, in solids, the maximum laser intensity reached is self-limited by the nonlinear interactions with the material [10–12]. This limitation can be understood in a very simple manner with the "lawnmower" model [12], in which the intensity above a certain threshold is absorbed by the material. The intensity leaving the interaction region is therefore, at maximum, equal to this threshold. The absorption is due to multiphoton ionization and electron avalanche. The plasma created defocuses the self-focusing beam, and a balance takes place, leading to filamentation [13]. By roughly assuming that the power in the filament is equal to the critical power for self-focusing P_{cr} and the intensity is limited to the breakdown threshold I_{br} [14], the typical radius of the filament will be given by $R_{fil} = [P_{cr}/\pi I_{br}]^{1/2} \approx 1.5\ \mu m$ ($P_{cr} = 2.6$ MW and $I_{br} \approx 2 \times 10^{13}$ W cm^{-2} in fused silica). This simple consideration suggests that there may be a regime where the beam profile becomes independent of the input energy, therefore increasing the control for the ablation of the films. We show that a more accurate modeling of the beam propagation gives the same order of magnitude of the confined radius after nonlinear interaction with the fused silica bulk.

*David.Rayner@nrc-cnrc.gc.ca
†Paul.Corkum@nrc-cnrc.gc.ca

 © 2014 American Physical Society

We concentrate on ultrathin polymer films on a dielectric substrate. We choose to work with polyelectrolyte films because their self-assembly as bilayers on surfaces is well understood and provides a way of producing uniform films of known thickness in a simple and reproducible manner [15]. The thickness is determined by the number of bilayers and can be controlled incrementally on a nanometer scale [16]. Polyelectrolyte films also have applications in sensing [17], and the ability to pattern them on a submicron scale is important from an applied perspective.

We show that substrate-mediated ablation is achievable with no substrate surface modification and that the size of the ablated film holes is almost independent of the laser energy on a wide processing window, therefore suppressing the deleterious effects of energy fluctuations. There is a sharp intensity threshold I_{th} for the ablation of these films [7]. Hence, the radius of the holes directly reflects the radius R_{th} of the beam at which the intensity is equal to I_{th}. We demonstrate how measuring the radius as a function of the position of the focal plane relative to the surface provides a new approach to profiling a tightly focused laser beam under nonlinear propagation conditions. We compare the profiles we measure with those predicted by a frequently applied model of nonlinear beam propagation. We show that the model reproduces well the tail of the beam profile in the range of laser energy investigated and can be used to estimate the size of the holes achievable by this technique.

II. EXPERIMENTAL SETUP

We use a Ti:sapphire laser delivering pulses of 45-fs duration (full width at half maximum, measured by frequency-resolved optical gating [18]) at 800-nm central wavelength. The repetition rate is fixed at 50 Hz. The energy is adjusted with the aid of a half-wave plate and a polarizing beam-splitter cube, and the pulse-to-pulse energy fluctuation is approximately 1.5% rms. The sample consists of a $25 \times 25 \times 0.22$-mm UV-grade fused silica coverslip, on which are deposited four bilayers of poly(allylamine hydrochloride) and poly(sodium 4-styrene-sulfonate) according to the layer-by-layer technique [15]. The 8-nm thickness of this deposit is an intrinsic property of the polyelectrolyte film, as confirmed by AFM measurements. The beam is focused by a 0.25-NA objective lens with a filling factor $\alpha = (a/w)^2 = 1$, where a is the lens aperture radius and w is the beam intensity radius at $1/e^2$ entering the objective. Dispersion induced by the various optical elements is compensated by prechirping the pulse. Single pulses are selected by an electromechanical shutter, and the sample is translated between each pulse to illuminate fresh material. We use AFM in tapping mode to characterize the morphology of the rear surface containing the film after irradiation.

We carefully measure *in situ* the beam radius by the knife-edge technique, as described in Ref. [7]. The results are presented in Fig. 1. While far from the focus the beam propagates as a Gaussian beam having a waist radius of 1.3 μm at $1/e^2$ of the peak intensity, the region near the focus is better fitted with a Gaussian beam of 1.9-μm waist radius. We attribute this behavior to the spherical aberrations of the objective lens as well as the lens overfilling that may induce a deviation from a pure Gaussian propagation [19]. When using our pulse with 200-nJ energy, the corresponding on-axis fluence at the focus under Gaussian beam propagation would be 3.5 J cm^{-2}.

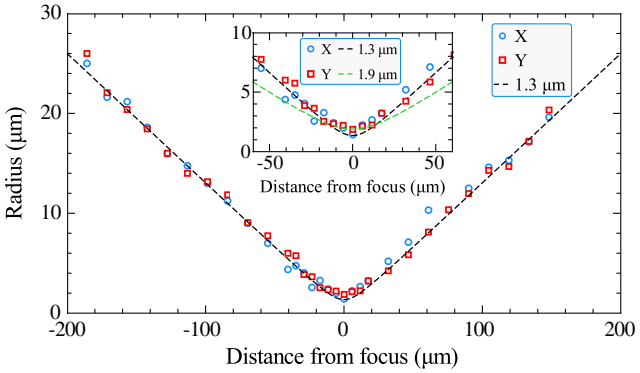

FIG. 1. Beam radius measured by the knife-edge technique in both orthogonal directions, when focused with the 0.25-NA microscope objective. Inset: Zoom close to the focal plane position. The dashed curves show the Gaussian radius for different waists.

III. RESULTS AND DISCUSSIONS

A. Substrate-mediated ablation

We first present (Fig. 2) AFM images of the polymer film surface and their corresponding depth cross sections after single-pulse irradiation with 200-nJ energy at two different focal positions. In Fig. 2(a), the focus is inside the fused silica substrate, 23.2 μm away from the rear surface. At this

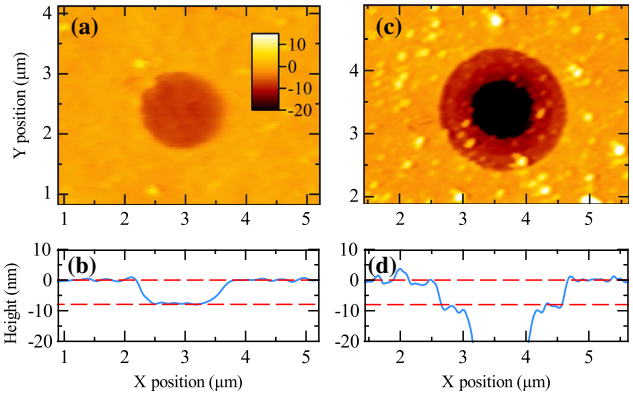

FIG. 2. AFM images of desorbed polymer film holes obtained with 200 nJ and (a) the focus 23.2 μm before the rear surface and (c) the focus 8.7 μm before the rear surface. The color bar indicates the height in nanometers. (b),(d) Corresponding cross sections. The dashed red lines indicate the depth of the film.

position, the cross section [Fig. 2(b)] reveals a sharp hole of 8-nm depth, with 1-μm diameter size, clearly indicating that only the film was removed while the substrate surface remained intact.

In Fig. 2(c), we position the focus only 8.7 μm away from the rear surface. There, the shape of the hole is different. It is composed of a central part of approximately 1-μm diameter and 70-nm depth surrounded by a ring of 2-μm outer diameter and 8-nm depth. While the deep center is caused by fused silica removal, the outer ring is due to the removal of the film only.

We then measure the radius of the ablated polymer as a function of the focal plane position for various laser energies. We move the focal plane with respect to the rear surface and record single-pulse beam widths with energies of 150, 200, and 500 nJ. We also apply 10 pulses with 55 nJ on one irradiation site for a non-self-focusing reference (diamond symbols in Fig. 3). We fit this last series with the radius R_{th} at which the intensity is equal to the threshold intensity $I_{\mathrm{th}} = 1.6 \times 10^{13}$ cm^{-2} of a Gaussian beam (black line) to locate the focus position [7] with a precision better than 7% of the Rayleigh range ($z_R = 20.9$ μm). In Fig. 3, the positive (negative) values of the horizontal axis correspond to the focal plane situated inside (outside) the substrate bulk.

When the focus is in the bulk, more than 26 μm away from the rear surface, the intensity at the surface is not sufficient to ablate the films for any pulse we study. As the focus approaches the surface, the tail of the pulse begins to interact with the film, and holes such as that in Fig. 2(a) are observed. With the focus even closer to the surface, the fused silica substrate is ablated as well, as seen in Fig. 2(c), until the focus moves out of the sample. In this region, only film ablation is observed again, but now there are large fluctuations. Eventually, the beam is fully transmitted when focused further out.

Figure 3 shows that between 10 and 26 μm, despite the large variation of energy (a factor of 3.3), the ablated film radius remains independent of energy, while the radius strongly depends on energy when the interaction is performed with the front of the pulse ($-55 < z < -20$ μm). As the large error bars show, film ablation is less reproducible in this region. This is because the interaction of the pulse with the bulk is minimized; therefore, intensity clamping does not occur. The intensity impinging on the film is close to the threshold, which makes ablation sensitive to laser energy fluctuations [7]. For 500 nJ, measurement is possible only away from the focus ($z \leq -23$ μm and $z \geq 0$ μm). Any closer, we find that the debris from fused silica ablation makes the AFM analysis impossible.

We study in more detail the region where the radius is independent of energy. In Fig. 4, we present a matrix of polymer film holes obtained with energies ranging from 150 to 190 nJ. Positioning the focal plane inside the substrate bulk, 23.2 μm away from the rear surface, leads to reproducible selective ablation of the film, with no substrate surface damage. For each energy, the sizes are randomly distributed about a mean value (the error bars in Fig. 3 represent the standard deviation over 20 measurements). In addition, increasing the energy by a factor of more than 3 has no significant influence on the ablation holes size within the error of measurement, despite the nonlinear nature of the interaction. This is evidenced in Fig. 5. For comparison, the radius R_{th} of a Gaussian beam

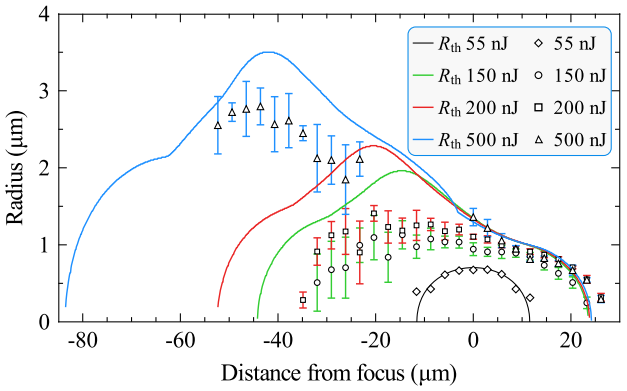

FIG. 3. Experimental radii (symbols) of ablated polymer film holes from the rear surface of a fused silica substrate as a function of focal plane position. Positive (negative) values of the horizontal axis correspond to the focal plane situated inside (outside) the substrate bulk. The solid lines show the calculated radius R_{th} for which the intensity is equal to the ablation threshold intensity ($I_{\mathrm{th}} = 1.6 \times 10^{13}$ W cm^{-2}) deduced from Gaussian propagation (55 nJ) and the model of wave propagation discussed in the text (150, 200, and 500 nJ).

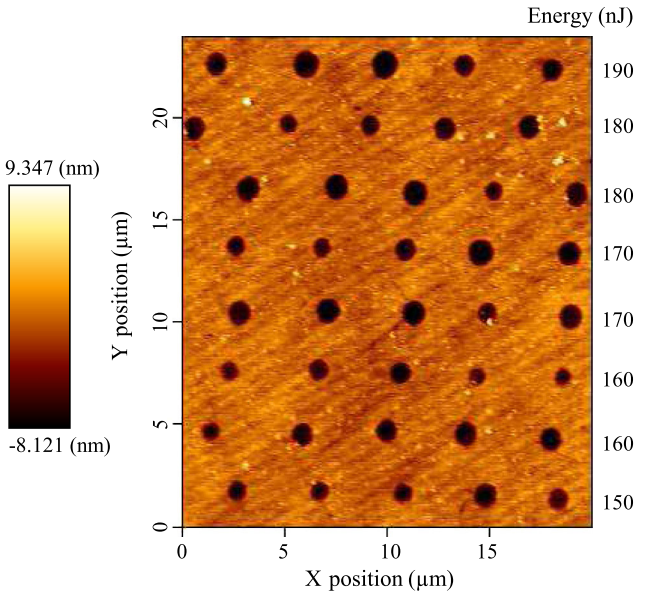

FIG. 4. AFM image of desorbed polymer holes, obtained by positioning the focal plane inside the dielectric bulk, 23.2 μm before the rear surface. For each row, the laser energy is indicated.

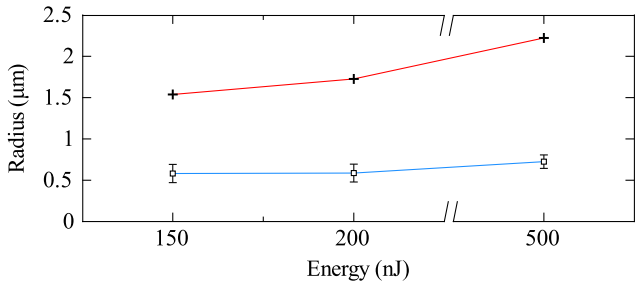

FIG. 5. When the laser focus is positioned in the fused silica bulk, 8.7 μm before the rear surface, the radius (half width at half maximum) of the ablated polymer film is almost independent of the incident energy (squares). Such is not the case with a Gaussian beam (cross symbols).

at which the intensity is $I_{\mathrm{th}} = 1.6 \times 10^{13}$ cm^{-2} at the same axial position would increase by 45% in this range of energy.

B. Beam profiling and comparison with model

Here, we make the link between the radius of the ablated film and the radius of the beam. The depth and the width of the central hole as seen in Fig. 2(b) fluctuate, while the outer ring is always 8 nm deep. Laser ablation of fused silica depends on many parameters, and the shape of the craters remains difficult to link to the beam profile. In addition, multiphoton ionization and the subsequent avalanche generation of electrons are highly nonlinear and can be enhanced in the presence of defects or color centers. In contrast, the thickness of the deposited films is well controlled and the films are uniform. The ablation of these films simply requires the intensity of the laser to be above the ablation threshold. This ablation threshold is lower than the threshold for nonlinear absorption in fused silica [7]. Therefore, in the ring-shaped region where only the film is removed, the fused silica substrate is transparent to the radiation. The radius of the ring is then equal to the beam radius R_{th} for which the intensity is the threshold intensity I_{th}, no matter how complex the interaction with fused silica is near the beam axis. Hence, the measured film hole radii in Fig. 3 will now be interpreted as the measured beam radii where the intensity is $I_{\mathrm{th}} = 1.6 \times 10^{13}$ cm^{-2}.

To get a better understanding of the physics of this substrate-mediated ablation, we now model [20] the propagation of the beam in fused silica by using the well-developed beam propagation model in a transparent medium [13,21–30]. The aim of these simulations is twofold. (i) Is it possible to account for the clamping of intensity observed in the tail of the pulse? (ii) Is the experimental beam profiling consistent with the model?

The model takes into account diffraction in the transverse plane, group-velocity dispersion (GVD), the instantaneous Kerr effect, plasma absorption and defocusing, photoionization using Keldysh's formalism [31], electron recombination, self-steepening, and space-time focusing [32].

We analyze the influence of the different terms and find that, in our conditions, GVD, self-steepening, and space-time focusing play negligible roles. Electron recombination is also not significant, mainly because the recombining electrons get trapped in an exciton state that is easy to reionize with the remaining part of the pulse via a four-photon transition only [33]. The experimental beam being well characterized, the adjustable parameters left are the nonlinear index of refraction n_2, the electron momentum transfer collision time τ_c that controls the balance between plasma absorption and plasma defocusing, and the generation of primary free carriers via photoionization.

The value of the nonlinear refractive index n_2 directly controls the importance of the Kerr effect in the model. We test the various values from the literature [34], looking at their influence on the radius for which the intensity is the ablation threshold intensity. With $n_2 = 3.75 \times 10^{-16}$ cm^2 W^{-1}, the critical power for self-focusing is $P_{\mathrm{cr}} \sim 1.8$ MW, which is reached with an energy of 85 nJ with our pulse. A lower value of $n_2 = 2.48 \times 10^{-16}$ cm^2 W^{-1} gives $P_{\mathrm{cr}} \sim 2.7$ MW and a corresponding energy of 130 nJ. For all following calculations we use $n_2 = 2.48 \times 10^{-16}$ cm^2 W^{-1}.

The electron momentum transfer collision time τ_c is another crucial parameter. It controls the balance between plasma absorption and plasma defocusing. There is no agreed-upon value in the literature, so it is usually adjusted arbitrarily. Arnold, Cartier, and DiMaria [35] calculate an energy-dependent collision time in the range 10^{-15}–10^{-16} s, and, more recently, Sun *et al.* measure a value of 1.7 fs [36]. We try different values of the damping term $\omega_0 \tau_c$ and fix it at 12 ($\tau_c = 5$ fs) to optimize agreement between modeled and experimental beam radii.

The model outputs intensity, fluence, and electron density as a function of time and space (see Supplemental Material [20]). From the peak intensity map, we extract the ablation threshold radius R_{th} as a function of focal position. The comparison between the experimental and the calculated radii is shown in Fig. 3. First, it is not possible to account for the experimental results with a non-self-focusing Gaussian propagation, except in the low-energy case (55 nJ) where the power is below the critical power for self-focusing and the intensity is below the ionization threshold. In the tail of the pulse ($0 < z < 25$ μm), the radius and the on-axis extent of film ablation would significantly change between 150 and 500 nJ with Gaussian beams. We measure that the radius is kept almost constant (Fig. 5) and that the on-axis extent differs by only 3 μm (Fig. 3), as opposed to 35 μm in the case of Gaussian beams. However, accepting that we treat n_2 and τ_c as adjustable parameters, the paraxial ray model reproduces this wavelength-scale feature quantitatively: The calculated beam profiles are independent of the input

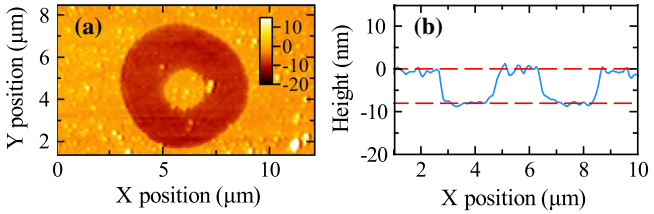

FIG. 6. (a) AFM image of desorbed polymer film holes obtained with 500 nJ and the focus 49.4 μm before the rear surface. The color bar indicates the height in nanometers. (b) Corresponding cross section. The dashed red lines indicate the depth of the film.

energy, and the experimental and calculated radii are relatively close. The model also predicts the on-axis position of the threshold intensity in the tail very well.

The front of the pulse is more subtle. We observe a strong dependence of the beam radius on input energy. This observation is not surprising, since nonlinear effects are less developed and pulse self-channeling has not yet started. However, the pulse does not ablate the film where it is expected, as seen by the large difference between the experimental and calculated radii. In addition, with a 200-nJ energy pulse, the model predicts a maximum electron density of approximately 2×10^{20} cm^{-3} located 30 μm before the focus. One would expect large substrate ablation with the surface at this position, but we do not even observe film removal. This deviation between model and experiment is attributed to the fact that the propagation is not purely Gaussian in our experiments, which is evidenced by the ring shape of the adsorbed film obtained at the front of the pulse for 500 nJ (Fig. 6). We attribute this to the slight overfilling of the microscope objective aperture in our experimental setup. The focusing of a truncated Gaussian beam evidences a dip in the center of the radial intensity distribution close to the focal plane [19]. Consistent with this explanation, we find that the dip disappears as the pulse energy is raised above the ablation threshold. We note that the size after focus is well reproduced, which means that, no matter the propagation of the beam before the focus, the nonlinear effects are dominant and strong enough to modify the propagation of the beam in the same way.

IV. CONCLUSION

In conclusion, we introduce a method allowing reproducible submicron ablation of thin films from a dielectric surface with a single femtosecond laser pulse. The method is robust and almost independent of the pulse energy in the range studied, providing a wide processing window for applications. The physics of nonlinear laser-dielectric interactions is accounted, within its limits, by a beam propagation model widely used in the field of filamentation. Applying the model in a semiempirical manner provides a good estimate of the size of holes achievable.

Figure 3 shows how our approach also allows the measurement of the spatial profile of a beam with submicron resolution and a high dynamical range. We have used it under high-intensity and tight-focus conditions where other techniques such as knife-edge profiling and array sensors are inapplicable. Even at low intensity, the technique can reveal more detail than the knife-edge method, as we have shown in Fig. 6 in the case of our own laser beam. While we use only one polymer, in future experiments, it should be possible to choose a series of polymer films with different ablation thresholds, thereby tracing out the profile of the self-focusing beam in more detail.

Therefore, substrate-mediated ablation provides an experimental method to investigate filamentation dynamics. One could, for instance, use the approach to characterize the filamentation of shaped beams or vectorial beams even where propagation is nonparaxial. While models have been developed that extend to nonparaxial propagation at high intensity, there has been no experimental method to test their assumptions. Using our technique in tighter focusing conditions to profile the beam should provide an experimental way to address the validity of these models.

ACKNOWLEDGMENTS

The authors are thankful to Dr. Y. Sultan for the deposition of the polymer films and Dr. M. Chen for assistance during AFM measurements. The authors also acknowledge the support of a Premier's Discovery Award grant.

[1] A. P. Joglekar, H. Liu, E. Meyhöfer, G. Mourou, and A. J. Hunt, Optics at critical intensity: Applications to nanomorphing, Proc. Natl. Acad. Sci. U.S.A. **101**, 5856 (2004).
[2] R. R. Gattass and E. Mazur, Femtosecond laser micromachining in transparent materials, Nat. Photonics **2**, 219 (2008).
[3] K. Sugioka and Y. Cheng, Ultrafast lasers—Reliable tools for advanced materials processing, Light Sci. Appl. **3**, e149 (2014).
[4] D. P. Banks, K. Kaur, and R. W. Eason, Influence of optical standing waves on the femtosecond laser-induced forward transfer of transparent thin films, Appl. Opt. **48**, 2058 (2009).
[5] S. Abreu Fernandes, B. Schoeps, K. Kowalick, R. Nett, C. Esen, M. Pickshaus, and A. Ostendorf, Femtosecond laser ablation of ITO/ZnO for thin film solar cells, Phys. Procedia **41**, 802 (2013).
[6] K. Kumar, K. KC Lee, J. Li, J. Nogami, N. P. Kherani, and P. R. Herman, Quantized structuring of transparent films with femtosecond laser interference, Light Sci. Appl. **3**, e157 (2014).
[7] L. Mercadier, J. Peng, Y. Sultan, T. A. Davis, D. M. Rayner, and P. B. Corkum, Femtosecond laser desorption of ultrathin

polymer films from a dielectric surface, Appl. Phys. Lett. **103**, 061107 (2013).

[8] H. Jeon, R. Schmidt, J. E. Barton, D. J. Hwang, L. J. Gamble, D. G. Castner, C. P. Grigoropoulos, and K. E. Healy, Chemical patterning of ultrathin polymer films by direct-write multiphoton lithography, J. Am. Chem. Soc. **133**, 6138 (2011).

[9] D. Grojo, M. Gertsvolf, H. Jean-Ruel, S. Lei, L. Ramunno, D. M. Rayner, and P. B. Corkum, Self-controlled formation of microlenses by optical breakdown inside wide-band-gap materials, Appl. Phys. Lett. **93**, 243118 (2008).

[10] A. Becker, N. Akozbek, K. Vijayalakshmi, E. Oral, C. M. Bowden, and S. L. Chin, Intensity clamping and re-focusing of intense femtosecond laser pulses in nitrogen molecular gas, Appl. Phys. B **73**, 287 (2001).

[11] W. Liu, S. Petit, A. Becker, N. Akzbek, C. M. Bowden, and S. L. Chin, Intensity clamping of a femtosecond laser pulse in condensed matter, Opt. Commun. **202**, 189 (2002).

[12] D. Rayner, A. Naumov, and P. Corkum, Ultrashort pulse non-linear optical absorption in transparent media, Opt. Express **13**, 3208 (2005).

[13] A. Couairon and A. Mysyrowicz, Femtosecond filamentation in transparent media, Phys. Rep. **441**, 47 (2007).

[14] N. Bloembergen, Laser-induced electric breakdown in solids, IEEE J. Quantum Electron. **10**, 375 (1974).

[15] Y. Sultan, R. Walsh, C. Monreal, and M. C. DeRosa, Preparation of functional aptamer films using layer-by-layer self-assembly, Biomacromolecules **10**, 1149 (2009).

[16] K. Ray, R. Badugu, and J. R. Lakowicz, Polyelectrolyte layer-by-layer assembly to control the distance between fluorophores and plasmonic nanostructures, Chem. Mater. **19**, 5902 (2007).

[17] P. Su and K. Cheng, Self-assembly of polyelectrolytic multilayer thin films of polyelectrolytes on quartz crystal microbalance for detecting low humidity, Sens. Actuators B **142**, 123 (2009).

[18] D. J. Kane and R. Trebino, Single-shot measurement of the intensity and phase of an arbitrary ultrashort pulse by using frequency-resolved optical gating, Opt. Lett. **18**, 823 (1993).

[19] Z. L. Horvath and Z. Bor, Focusing of truncated Gaussian beams, Opt. Commun. **222**, 51 (2003).

[20] See Supplemental Material at http://link.aps.org/supplemental/10.1103/PhysRevApplied.2.034001 for a description of the model.

[21] A. Braun, G. Korn, X. Liu, D. Du, J. Squier, and G. Mourou, Self-channeling of high-peak-power femtosecond laser pulses in air, Opt. Lett. **20**, 73 (1995).

[22] A. Couairon and L. Bergé, Light filaments in air for ultraviolet and infrared wavelengths, Phys. Rev. Lett. **88**, 135003 (2002).

[23] S. L. Chin, T.-J. Wang, C. Marceau, J. Wu, J. S. Liu, O. Kosareva, N. Panov, Y. P. Chen, J.-F. Daigle, S. Yuan, A. Azarm, W. W. Liu, T. Seideman, H. P. Zeng, M. Richardson, R. Li, and Z. Z. Xu, Advances in intense femtosecond laser filamentation in air, Laser Phys. **22**, 1 (2012).

[24] A. Dubietis, A. Couairon, E. Kucinskas, G. Tamosauskas, E. Gaizauskas, D. Faccio, and P. Di Trapani, Measurement and calculation of nonlinear absorption associated with femtosecond filaments in water, Appl. Phys. B **84**, 439 (2006).

[25] V. Jukna, G. Tamoauskas, G. Valiulis, M. Aputis, M. Puida, F. Ivanauskas, and A. Dubietis, Filamentation of ultrashort light pulses in a liquid scattering medium, Appl. Phys. B **94**, 175 (2009).

[26] S. Tzortzakis, L. Sudrie, M. Franco, B. Prade, A. Mysyrowicz, A. Couairon, and L. Bergé, Self-guided propagation of ultrashort IR laser pulses in fused silica, Phys. Rev. Lett. **87**, 213902 (2001).

[27] L. Sudrie, A. Couairon, M. Franco, B. Lamouroux, B. Prade, S. Tzortzakis, and A. Mysyrowicz, Femtosecond laser-induced damage and filamentary propagation in fused silica, Phys. Rev. Lett. **89**, 186601 (2002).

[28] Z. Wu, H. Jiang, Q. Sun, H. Yang, and Q. Gong, Filamentation and temporal reshaping of a femtosecond pulse in fused silica, Phys. Rev. A **68**, 063820 (2003).

[29] A. Couairon, L. Sudrie, M. Franco, B. Prade, and A. Mysyrowicz, Filamentation and damage in fused silica induced by tightly focused femtosecond laser pulses, Phys. Rev. B **71**, 125435 (2005).

[30] I. M. Burakov, N. M. Bulgakova, R. Stoian, A. Mermillod-Blondin, E. Audouard, A. Rosenfeld, A. Husakou, and I. V. Hertel, Spatial distribution of refractive index variations induced in bulk fused silica by single ultrashort and short laser pulses, J. Appl. Phys. **101**, 043506 (2007).

[31] L. V. Keldysh, Ionization in the field of a strong electromagnetic wave, Sov. Phys. JETP **20**, 1307 (1965).

[32] J. E. Rothenberg, Space-time focusing: Breakdown of the slowly varying envelope approximation in the self-focusing of femtosecond pulses, Opt. Lett. **17**, 1340 (1992).

[33] D. Grojo, M. Gertsvolf, S. Lei, T. Barillot, D. M. Rayner, and P. B. Corkum, Exciton-seeded multiphoton ionization in bulk SiO_2, Phys. Rev. B **81**, 212301 (2010).

[34] David Milam, Review and assessment of measured values of the nonlinear refractive-index coefficient of fused silica, Appl. Opt. **37**, 546 (1998).

[35] D. Arnold, E. Cartier, and D. J. DiMaria, Acoustic-phonon runaway and impact ionization by hot electrons in silicon dioxide, Phys. Rev. B **45**, 1477 (1992).

[36] Q. Sun, H. Jiang, Y. Liu, Z. Wu, H. Yang, and Q. Gong, Measurement of the collision time of dense electronic plasma induced by a femtosecond laser in fused silica, Opt. Lett. **30**, 320 (2005).